

Received: 2020.03.07

Accepted: 2020.04.10

Available online: 2020.05.22

Published: 2020.07.07

# Self-Assembling Peptide Scaffold Carrying Neural-Cell Adhesion Molecule-Derived Mimetic-Peptide Transplantation Promotes Proliferation and Stimulates Neurite Extension by Modulating Tau Phosphorylation and Calpain/Glycogen Synthase Kinase 3 beta (GSK-3 $\beta$ ) in Neurons

Authors' Contribution:  
Study Design A  
Data Collection B  
Statistical Analysis C  
Data Interpretation D  
Manuscript Preparation E  
Literature Search F  
Funds Collection G

BCDEF 1 **Jian Xu\***  
BCDF 2 **Jing Feng\***  
BCD 1 **Yu-dong Liu**  
BCF 1 **Tao Hu**  
BF 1 **Ming-jing Li**  
ACDEG 1 **Fan Li**

1 Department of Pediatric Orthopedics, Wuhan Fourth Hospital (Puai Hospital), Tongji Medical College, Huazhong University of Science and Technology, Wuhan, Hubei, P.R. China

2 Nursing Department, Wuhan Fourth Hospital (Puai Hospital), Tongji Medical College, Huazhong University of Science and Technology, Wuhan, Hubei, P.R. China

\* Jian Xu and Jing Feng are the co first author and contributed equally to this study

Fan Li, e-mail: 349401236@qq.com

Corresponding Author:

Source of support:

Departmental sources

**Background:** Self-assembling peptide scaffolds have been extensively applied in tissue engineering. Many investigations have modified self-assembling peptide scaffolds by integrating functional motifs, with promising applications. This study aimed to generate a novel RADA16 self-assembling peptide scaffold integrating a neural-cell adhesion molecule-derived mimetic-peptide (SIDRVEPYSSTAQ) and evaluated the effects on neuron proliferation.

**Material/Methods:** A 37-amino-acids peptide of RADA16-activation motif containing neural-cell adhesion molecule-derived mimetic-peptide (SIDRVEPYSSTAQ) was synthesized and self-assembled into a scaffold. Dorsal root ganglion (DRG) and spinal cord motor neurons (SCMN) were primarily isolated and identified. Neurons (DRG and SCMN) were divided into FRM, FRM-MP, and FRM-MP-LiCl groups. The adherence ability of neurons was evaluated using toluidine blue staining. Proliferation and apoptosis of neurons were assessed using CCK-8 and flow cytometry assay, respectively. Immunofluorescence assay was used to measure neurite extension. Western blot assay was used to assess GSK-3 $\beta$ /p-GSK-3 $\beta$ , Tau/p-Tau, and calpain expression in neurons.

**Results:** FRM-MP-LiCl released multiple-peptide with higher efficiency. FRM-MP-LiCl significantly enhanced proliferation and inhibited apoptosis compared to FRM and FRM-MP groups ( $p < 0.05$ ). FRM-MP-LiCl incubation increased adherent ability compared to the FRM and FRM-MP groups ( $p < 0.05$ ). FRM-MP-LiCl remarkably increased neurite length ( $p < 0.05$ ), numbers ( $p < 0.05$ ), and branches. FRM-MP-LiCl significantly reduced GSK-3 $\beta$  phosphorylation (p-GSK-3 $\beta$ /GSK-3 $\beta$ ) and Tau phosphorylation (p-Tau/Tau) compared to the FRM and FRM-MP groups ( $p < 0.05$ ). FRM-MP-LiCl significantly downregulated calpain compared to the FRM and FRM-MP groups ( $p < 0.05$ ).

**Conclusions:** The generated self-assembling peptide scaffold carrying FRM motif (SIDRVEPYSSTAQ) promoted neuron proliferation and adherent ability, inhibited apoptosis, and stimulated neurite extension, by reducing Tau protein phosphorylation through the calpain/GSK-3 $\beta$  signaling pathway.

**MeSH Keywords:** Cell Adhesion Molecules, Neuron-Glia • Peptide Fragments • Tissue Engineering • Tissue Scaffolds

**Full-text PDF:** <https://www.annalsoftransplantation.com/abstract/index/idArt/924093>



3368



8

38



## Background

Peptides are an important topic in the biomedical field and have been extensively proven to be an ideal therapeutic strategy for many diseases [1,2]. Peptides are used in the treatment of cancers [3], diabetes [4], and cerebrovascular disorders [5]. However, they are easily cleaved by circulating proteases and thus are short-lived [6]. In order to resolve this problem, peptides must be carried with a delivery vehicle with “on-demand” release cues (such as proteolytic cleavage sites) [7]. The synthetic peptide vehicle or peptide scaffold with intrinsic functional domains can exploit properties of the natural molecule/peptides to the cellular targeting regions [8]. Therefore, it is critical to generate an ideal and novel peptide scaffold.

Self-assembling peptides have been generated to spontaneously assemble into a scaffolding material by forming electrostatic interactions, hydrogen bonds, and Van-der-Waals forces (non-covalent) [9]. Self-assembling peptide scaffolds can promote wound-healing, bone regeneration, and drug delivery [10,11]. Self-assembling peptide scaffolds demonstrate good biocompatibility and can be completely degraded without any toxic products [12]. The (arginine-alanine-aspartate-alanine)<sub>4</sub> or (RADA)<sub>4</sub> or RADA16 has been synthesized as an appropriate self-assembling peptide candidate for molecular programming [13,14]. The RADA16 peptide system has been applied in tissue engineering and tissue repair based on the release characteristics of peptides or drugs [13].

A previous study [15] reported that RADA16 peptide can mimic the growing microenvironment and promote the proliferation of cells, but the effects on growth of neurons have not been fully clarified. In this study, we synthesized a 37-aminoacids peptide, RADA16-activation motif (RADA16-FRM) (AcN-AAAGG GDDSIDRVEPYSSTAQRADARADARADARA DA-CONH<sub>2</sub>), containing neural cell adhesion molecule (NCAM)-derived mimetic-peptide (MP) (SIDRVEPYSSTAQ), which can self-assemble into the nano-fiber scaffold. In this study, MP (SIDRVEPYSSTAQ) was coupled and fused at the N-terminal, which is not consistent with a previous study describing 31-amino acid peptide RADA-FRM (AcN-RADARADARADARADAGGSIDRVE PYSSTAQ) sequence containing NCAM-derived peptide [16]. If RADA16 is also fused at the N-terminal, MP might affect the self-assembly of RADA16. Therefore, we did not fuse the RADA16 sequence at the C-terminal. In this study, RADA16 peptide containing SIDRVEPYSSTAQ were utilized to investigate the effects on the biology of neurons.

## Material and Methods

### Peptide generation and purification

The single FRM peptide, neural-cell adhesion molecule-derived mimetic-peptide, sequence was SIDRVEPYSSTAQ. The FRM-MP peptide sequence (containing RADA16 peptide: RADARADARADARADA and NCAM-derived MP: SIDRVEPYSSTAQ) was AcN-AAGGGDDSIDRVEPYSS TAQRADARADARADARADA-CONH<sub>2</sub>. In the above RADA16-FRM-MP peptide, the sequence (-AAAGGGDD-) was added at the N-terminal. This sequence has a synergistic effect with MP (SIDRVEPYSSTAQ), but it makes the MP at the back extend to the fiber surface. Therefore, the addition of this sequence can expose the active area of MP (SIDRVEPYSSTAQ). FRM and FRM-MP were commercially synthesized by Western Biotech (Chongqing, China). The N-terminus of these 2 peptides was acetylated and the C-terminus of these 2 peptides was amidated in this study. Both peptides were also purified using the HPLC method and characterized using mass-spectroscopy. The final purity of FRM and FRM-MP was 90.00% and 90.39%, respectively.

### Cell isolation, primary culture, and identification

Wistar rats (Western Biotech., Chongqing, China) were anesthetized using pentobarbital at a dosage of 50 mg/kg body weight and fixed in prone position. The dorsal root ganglion (DRG) cells isolation and primary culture were conducted according to the method described in a previous study [17]. The DRG cells were identified by staining with the rabbit anti-rat choline acetyltransferase (ChAT) antibody (cat. no. ab85609, Abcam Biotech., Cambridge, MA, USA), using immunocytochemistry assay as described elsewhere. The spinal cord motor neuron (SCMN) cells were isolated and primarily maintained as previously reported [18]. The SCMN cells were identified by staining with rabbit anti-rat neuron-specific enolase (NSE) (cat. no. ab53025, Abcam Biotech), using immunocytochemistry assay as described elsewhere. Briefly, both DRG and SCMN cells were cultured in DMEM (Gibco BRL Co., Grand Island, NY, USA) containing 10% FBS (Gibco BRL Co.) at 37°C and 5% CO<sub>2</sub>.

The animal experiments were approved by the Institutional Animal Care and Use Committee of Wuhan Fourth Hospital (Puai Hospital), Tongji Medical College, Huazhong University of Science and Technology, Wuhan, China.

### Trial grouping and peptide/LiCl release detection

In this study, 3 groups – the DRG and SCMN cells incubated with FRM group (FRM group), the DRG and SCMN cells incubated with FRM-MP group (FRM-MP group), and the DRG and SCMN cells incubated with FRM-MP and LiCl group (FRM-MP-LiCl group). The cells in the DRG and SCMN cells in FRM group

were incubated with FRM peptide at a dosage of 2 mg/ml in DMEM medium solution containing 10% FBS at 37°C and 5% CO<sub>2</sub> in 6-well plates. Cells of the DRG and SCMN cells in FRM-MP group were incubated with FRM-MP peptide at a dosage of 2 mg/ml in DMEM solution containing 10% FBS at 37°C and 5% CO<sub>2</sub> in 6-well plates. Cells in the DRG and SCMN cells in FRM-MP group were incubated with FRM-MP peptide at a dosage of 2 mg/ml and LiCl at dosage of 1 mg/ml in DMEM solution containing 10% FBS at 37°C and 5% CO<sub>2</sub> in 6-well plates.

For the self-assembled peptide RADA-16, which is a nano-material synthesized by chemical synthesis, the RADA-16 solution can be rapidly assembled into nano-fiber hydrogel under the excitation of salt solution. LiCl is dissociated into lithium iNOS automatically in water, which can be bound to polypeptides containing carboxyl groups. This process does not need the participation of cells. The release of MP was detected using an atomic absorption spectrophotometer (cat. no. CASCQYS-A0007). The release of LiCl was detected using inductively coupled plasma mass spectrometry (cat. no. CASCQYS-A0004).

#### **Toluidine blue staining**

Cells were digested with 0.2% trypsin (Beyotime Biotech, Shanghai, China), re-suspended with DMEM (Gibco BRL Co.), and the cell density was adjusted to 2×10<sup>4</sup>/ml. In 12-well plates, the cell climbing pieces (round pieces) were placed. The cell suspension was dropped onto the pieces and cultured for 30 min. Then, DMEM containing 10% FBS was added to 12-well plates and cultured at 37°C and 5% CO<sub>2</sub> in an incubator for 24 h. The pieces were washed using PBS (ZSGB-Bio., Beijing, China) 3 times (5 min per time) and incubated with 4% paraformaldehyde (Beyotime Biotech) at room temperature for 20 min. Subsequently, the cells on pieces were stained using toluidine blue (Leagene Biotech Co., Beijing, China) for 5 min and rinsed with PBS for 30 s. Finally, the pieces were air-dried naturally and sealed with neutral gum and observed under microscopy (Mode: BX51, Olympus, Tokyo, Japan).

#### **Cell Counting Kit-8 (CCK-8) assay**

The cell survivals in this study were analyzed using CCK-8 kit (cat. no. 96992, Sigma-Aldrich, St. Louis, MO, USA) according to the protocol of the manufacturer. Briefly, the cells were adjusted to a density of 1×10<sup>5</sup>/ml, seeded into 96-well plates (100 μ per well) and cultured for 24 h at 37°C and 5% CO<sub>2</sub>. Then, 10 μl CCK-8 reagent was added into each well and cultured for 4 h at 37°C. The absorbance of each well was measured with an ELISA reader (Thermo Fisher Scientific, Hudson, NH, USA) at a wavelength of 450 nm.

#### **Flow cytometry assay for measuring apoptosis**

The cells were seeded into a 6-well plate and cultured to 70% confluence. Cells were seeded into a centrifuge tube and centrifuged for 5 min at 2000 r/min, and then washed with PBS and centrifuged again at 2000 r/min again for 5 min. Then, 1×10<sup>5</sup> cells were collected and incubated with 5 μl 7-ADD staining solution for 15 min at room temperature in the dark. A total of 1 μl Annexin V-PE was also added into the cells and incubated for 15 min at room temperature in the dark. The staining methods for both 7-ADD and Annexin V-PE were conducted following the protocol of the Annexin V-PE/7-ADD Apoptosis Detection Kit (cat. no. 559763, BD Biosciences, Franklin Lakes, NJ, USA). Finally, the stained cells were examined using a flow cytometer within 60 min.

#### **Immunofluorescence assay for measuring neurite extension**

Neurons were traced with the neurofilament protein 200 (NF200) immunoreactivity to visualize the neurites. In brief, after several passages and cultures of isolated neurons, including DRG and SCMN, which were treated with FRM, FRM-MP, or FRM-MP-LiCl and incubated with rabbit anti-rat NF200 polyclonal antibody (cat. no. ab204893, Abcam Biotech, Cambridge, MA, USA) at 4°C overnight for the immunofluorescence assays. Then, the neurons were incubated using the Alexa Fluor 488-labeled goat anti-rabbit IgG (cat. no. ab150077, Abcam Biotech.) at 37°C for 30 min in the dark. After immunostaining, the images and tracing of the neurite (length, number, and branching) were captured using a laser confocal fluorescence microscope (Model: TCS SP5, Leica, Frankfurt, Germany). The average length of SCMN and DRG neurons was calculated with imaging analysis software (version: QWin-V3, Leica, Frankfurt, Germany).

#### **Western blot assay**

All of the DRG and SCMN neurons were harvested at 24 h after culturing and were lysed in lysis buffer (Sangon Biotech Co., Shanghai, China). The cell lysates were centrifuged at 10 000 r/min at 4°C for 30 min to obtain proteins, and concentrations were measured using the BCA Protein Assay Kit (cat. no. P0010S, Beyotime Biotech, Shanghai, China). The lysates were subjected to the SDS-PAGE, and the separated proteins in gels were electro-transferred onto the PVDF membrane (Bio-Rad Laboratories, Hercules, CA, USA). Then, the PVDF membranes were washed with phosphate-buffered saline tween-20 (PBST) solution 3 times (5 min per time) and incubated with mouse anti-rat GSK-3β monoclonal antibody (cat. no. ab93926, 1: 2000), rabbit anti-rat p-GSK-3 (α+β) (Y216+Y279) monoclonal antibody (cat. no. ab68476; 1: 2000), rabbit anti-rat Tau monoclonal antibody (cat. no. ab32057; 1: 2000), rabbit

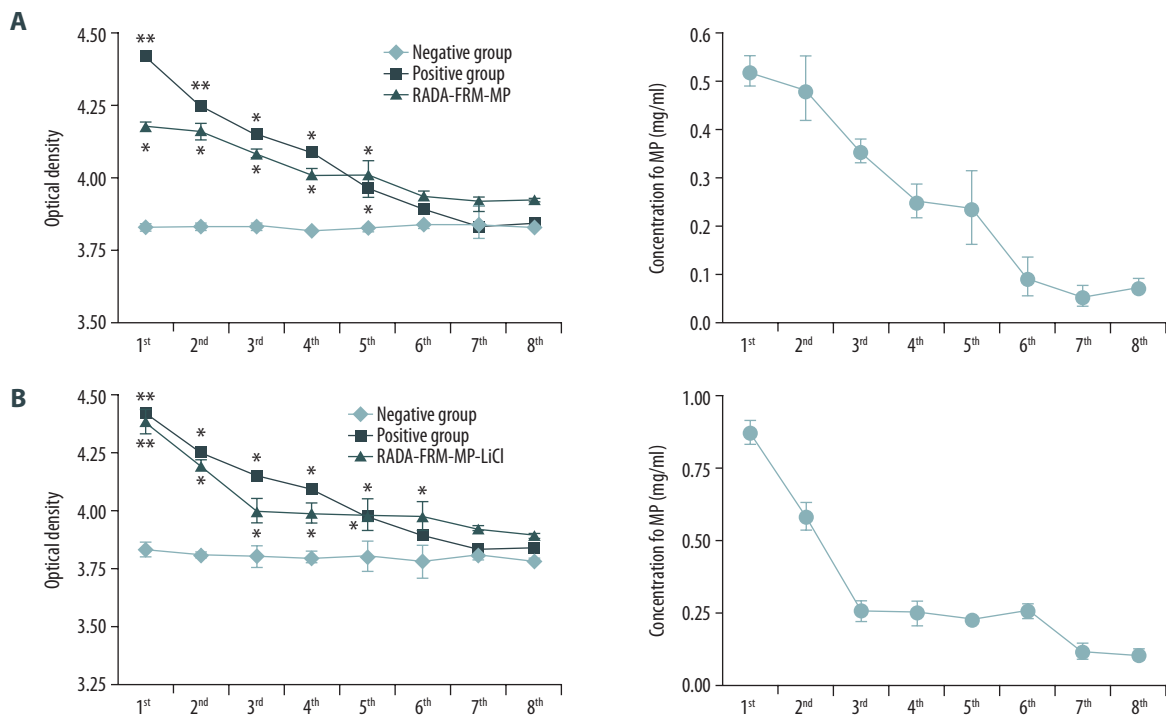


**Figure 1.** Multiple peptide release curves of RADA16-FRM-MP and RADA16-FRM-MP-LiCl-incubated neurons from the 1<sup>st</sup> day to the 8<sup>th</sup> day. (A) Release curves for RADA16-FRM-MP-incubated neurons from the 1<sup>st</sup> day to the 8<sup>th</sup> day. (B) Release curves for RADA16-FRM-MP-LiCl-incubated neurons from the 1<sup>st</sup> day to the 8<sup>th</sup> day. \*  $p < 0.05$ , \*\*  $p < 0.01$  vs. Negative group.

anti-rat p-Tau S416 polyclonal antibody (cat. no. ab119391; 1: 1000), rabbit anti-rat calpain 1 monoclonal antibody (cat. no. ab108400; 1: 2000), and rabbit anti-rat GAPDH polyclonal antibody (cat. no. ab9485; 1: 1000) at 4°C overnight. The primary antibodies-stained PVDF membranes were washed with PBST 3 times, 5 min per time. Subsequently, PVDF membranes were incubated using HRP-labeled goat anti-mouse IgG (cat. no. ab205719; 1: 1000) and HRP-labeled goat anti-rabbit IgG (cat. no. ab97051; 1: 1000) at room temperature for 2 h. All of the above primary and secondary antibodies were purchased from Abcam Biotech (Cambridge, MA, USA). The above immuno-blot in PVDF membranes were developed using ECL chemiluminescence Western Blotting Substrate (cat. no. 32109, Thermo Scientific Pierce, Rockford, IL, USA) and captured using the Gel-Imaging System (Model: Tannon-4200, Tannon Sci. Tech. Co., Shanghai, China). Finally, the images of immuno-blot were scanned and analyzed with Labworks™ Analysis Software (version: 4.0, Labworks, Upland, CA, USA).

### Statistical analysis

Data are expressed as mean±standard deviation (SD). The professional SPSS software 20.0 (SPSS, Inc., Chicago, USA) was employed for analyzing the differences between groups. The differences were assessed by ANOVA followed by post hoc Tukey

test between groups at the same time points. P value less than 0.05 was defined as statistically significant.

## Results

### RADA16-FRM-MP-LiCl released multiple peptides with higher efficiency

In this study, the optical density of cell culture supernatant was measured. The results showed that the optical density values of the RADA-FRM-MP group and Positive group were significantly higher compared to that of the Negative group, from the 1<sup>st</sup> day to 5<sup>th</sup> day after peptide administration (Figure 1A,  $p < 0.05$ ). The amount of peptide released from cells in RADA-FRM-MP group was the highest on the first day of culture (0.5228 mg/ml), and the peptide concentration gradually decreased over time (Figure 1A). Optical density values of the RADA-FRM-MP-LiCl group were also significantly higher compared to that of the Negative group from the 1<sup>st</sup> day to 6<sup>th</sup> day after FRM peptide and LiCl administration (Figure 1B,  $p < 0.05$ ). The amount of peptide released from cells in the RADA-FRM-MP-LiCl group peaked on the 1<sup>st</sup> day after culture (0.8206 mg/ml), and peptide concentration gradually decreased over time (Figure 1B).

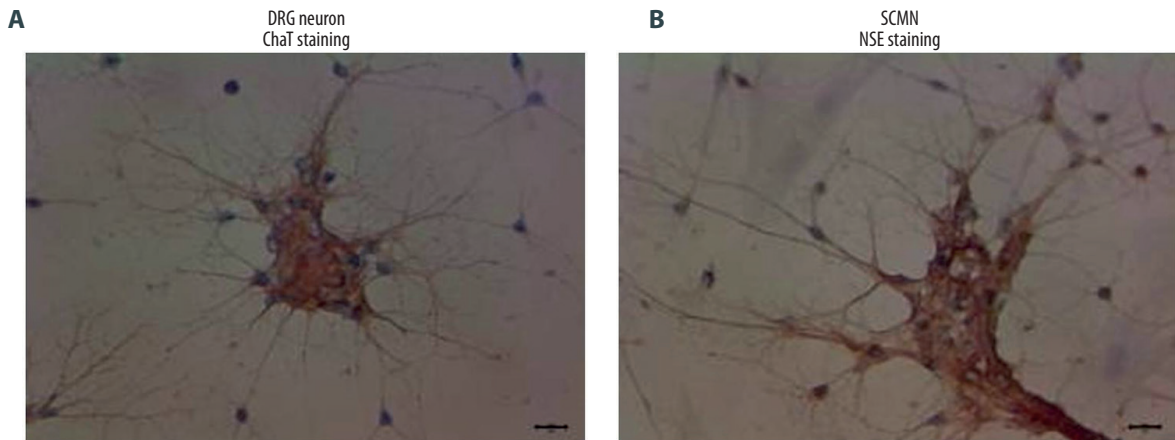


**Figure 2.** Identification of DRG cells (A) and SCMN cells (B) using immunocytochemistry assay. The DRG cells were identified by detecting the ChAT molecule. SCMN cells were identified by detecting the NSE molecule.

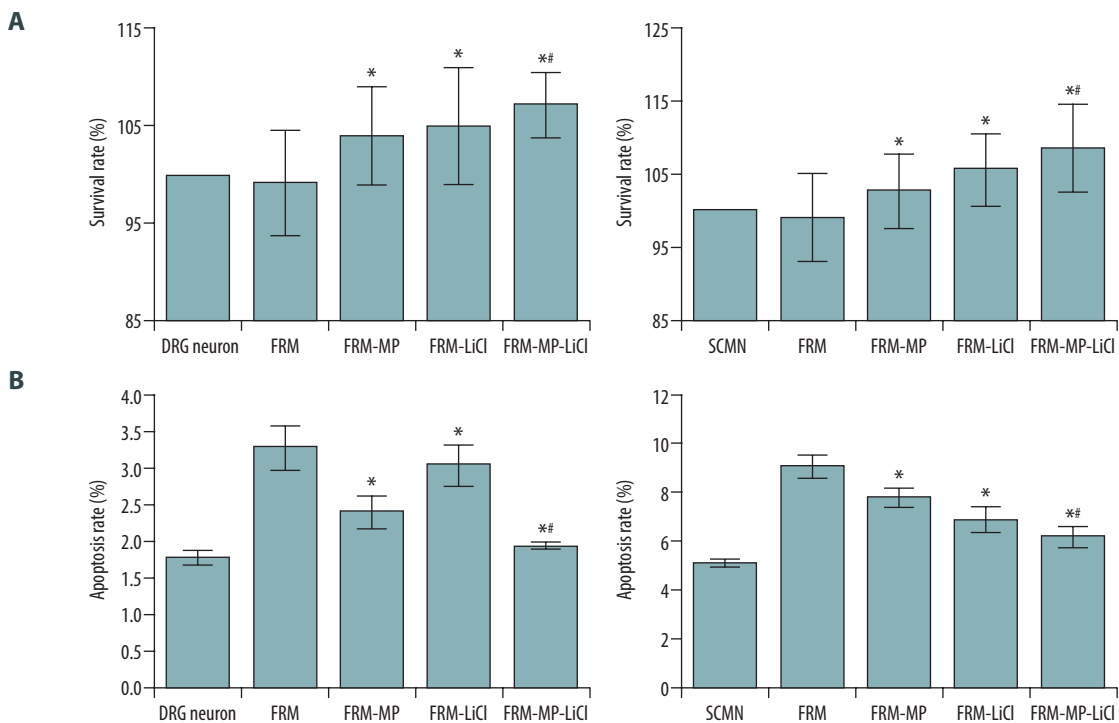


**Figure 3.** Evaluation of proliferation and apoptosis of neurons in different groups. (A) Determination for the survival rates of DRG and SCMN neurons using MTT assay in FRM, FRM-MP, FRM-LiCl, and FRM-MP-LiCl groups. (B) Determination of apoptosis of DRG and SCMN neurons using flow cytometry assay in FRM, FRM-MP, FRM-LiCl, and FRM-MP-LiCl groups. Apoptosis rate, calculated as early apoptosis rate plus late apoptosis. \*  $p < 0.05$  vs. FRM group. #  $p < 0.05$  vs. FRM-MP group.

### RADA16-FRM-MP-LiCl increased proliferation and inhibited apoptosis

We determined the cell proliferation and apoptosis of primarily cultured DRG and SCMN cells. The DRG cells (Figure 2A) and SCMN cells (Figure 2B) were successfully cultured and identified.

The CCK-8 findings indicated that FRM-MP and FR-MP-LiCl significantly increased the survival rates in DRG and SCMN cells compared with that in the FRM group (Figure 3A,  $p < 0.05$ ). Meanwhile, the survival rate of cells in the FRM-MP-LiCl group was remarkably higher than in the FRM-MP group (Figure 3A,  $p < 0.05$ ). Flow cytometry assay showed that FRM-MP and FR-MP-LiCl incubation

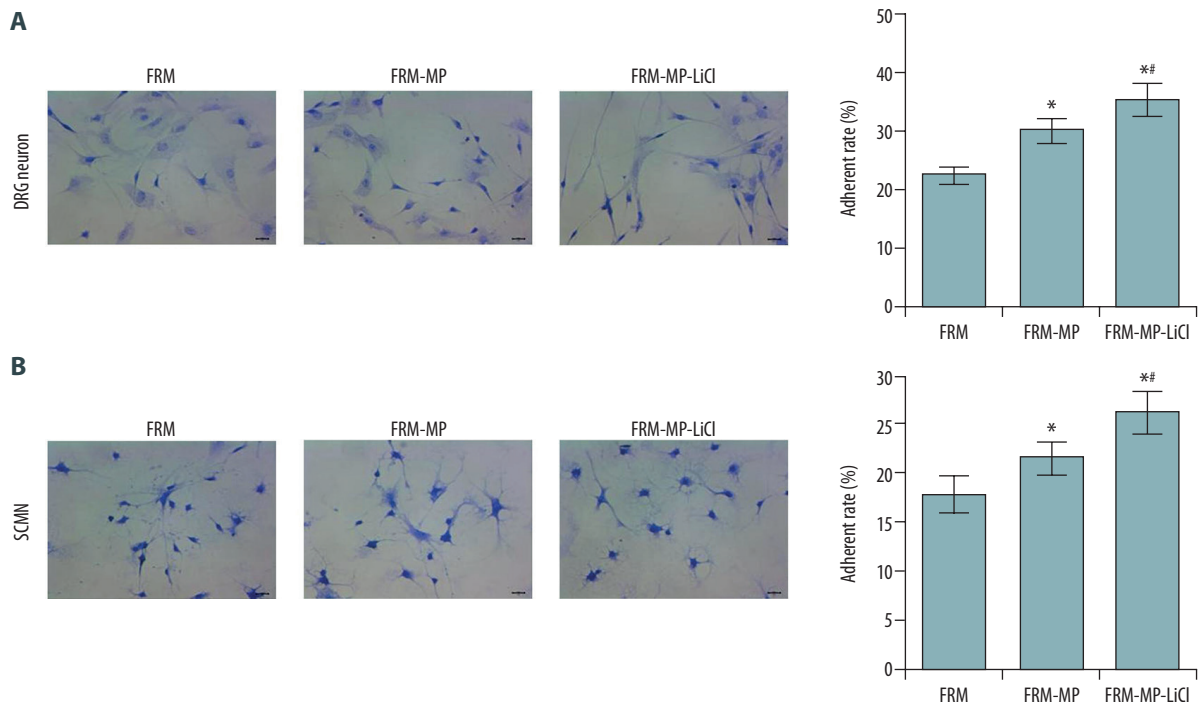


**Figure 4.** Effects of FRM-MP on the adherent ability of neurons determined using toluidine blue staining. (A) Evaluation of the effect of FRM-MP on the adherent ability of DRG neurons. (B) Evaluation of the effect of FRM-MP on the adherent ability of SCMN neurons. The blue-stained cells represent the adherent cells. \*  $p < 0.05$  vs. FRM group. #  $p < 0.05$  vs. FRM-MP group.

significantly decreased survival rates of DRG and SCMN cells compared with the FRM group (Figure 3B,  $p < 0.05$ ). The survival rate of cells in the FRM-MP-LiCl group was significantly lower than in the FRM-MP group (Figure 3A,  $p < 0.05$ ).

#### RADA16-FRM-MP-LiCl incubation increased adherent ability of cells

The results showed that the adherent ability of DRG cells in the FRM-MP-LiCl and FRM-MP incubation group was significantly increased compared to that in the FRM group (Figure 4A,  $p < 0.05$ ). Also, DRG cells in the FRM-MP-LiCl group demonstrated significantly higher adherent rate compared with that in the FRM-MP group (Figure 4A,  $p < 0.05$ ), and adherent rates were also significantly enhanced in SCMN (Figure 4B) cells in the FRM-MP-LiCl and FRM-MP incubation group compared to that in the FRM group ( $p < 0.05$ ). SCMN cells in the FRM-MP-LiCl group had remarkably higher adherent rates comparing to that in the FRM-MP group (Figure 4B,  $p < 0.05$ ).

#### RADA16-FRM-MP-LiCl increased neurite length and number of neurons

The length and number of neurites in DRG and SCMN neurons were determined using immunofluorescence assay (Figure 5A). The statistical analysis indicated that neurite length of DRG

and SCMN neurons in the FRM-MP-LiCl and FRM-MP groups was significantly longer compared to that in the FRM group (Figure 5B,  $p < 0.05$ ). Meanwhile, the neurite length of DRG and SCMN neurons in the FRM-MP-LiCl group was significantly longer compared to that in the FRM-MP group (Figure 5B,  $p < 0.05$ ), and there were more neurites in DRG and SCMN neurons in the FRM-MP-LiCl and FRM-MP groups compared to that in the FRM group (Figure 5C,  $p < 0.05$ ). Neurons in the FRM-MP-LiCl and FRM-MP groups had obviously more neurite branches than in the FRM group (Figure 5A). Importantly, neurons in the FRM-MP-LiCl group had the longest, most branched, and most abundant neurites (Figure 5A).

#### RADA16-FRM-MP-LiCl reduced phosphorylation of GSK-3 $\beta$

The GSK-3 $\beta$  signaling pathway was examined using Western blot assay (Figure 6A). The results indicated that FRM-MP-LiCl incubation significantly reduced the ratio of p-GSK-3 $\beta$ /GSK-3 $\beta$  in DRG neurons compared to that in the FRM group and FRM-MP group (Figure 6B,  $p < 0.05$ ). FRM-MP-LiCl administration also remarkably decreased the ratio of p-GSK-3 $\beta$ /GSK-3 $\beta$  in SCMN neurons compared to that in the FRM group and FRM-MP group (Figure 6C,  $p < 0.05$ ). Although FRM-MP obviously downregulated p-GSK-3 $\beta$ /GSK-3 $\beta$  in DRG (Figure 6B) and SCMN (Figure 6C) neurons compared with the FRM group, the differences were not significant ( $p > 0.05$ ).

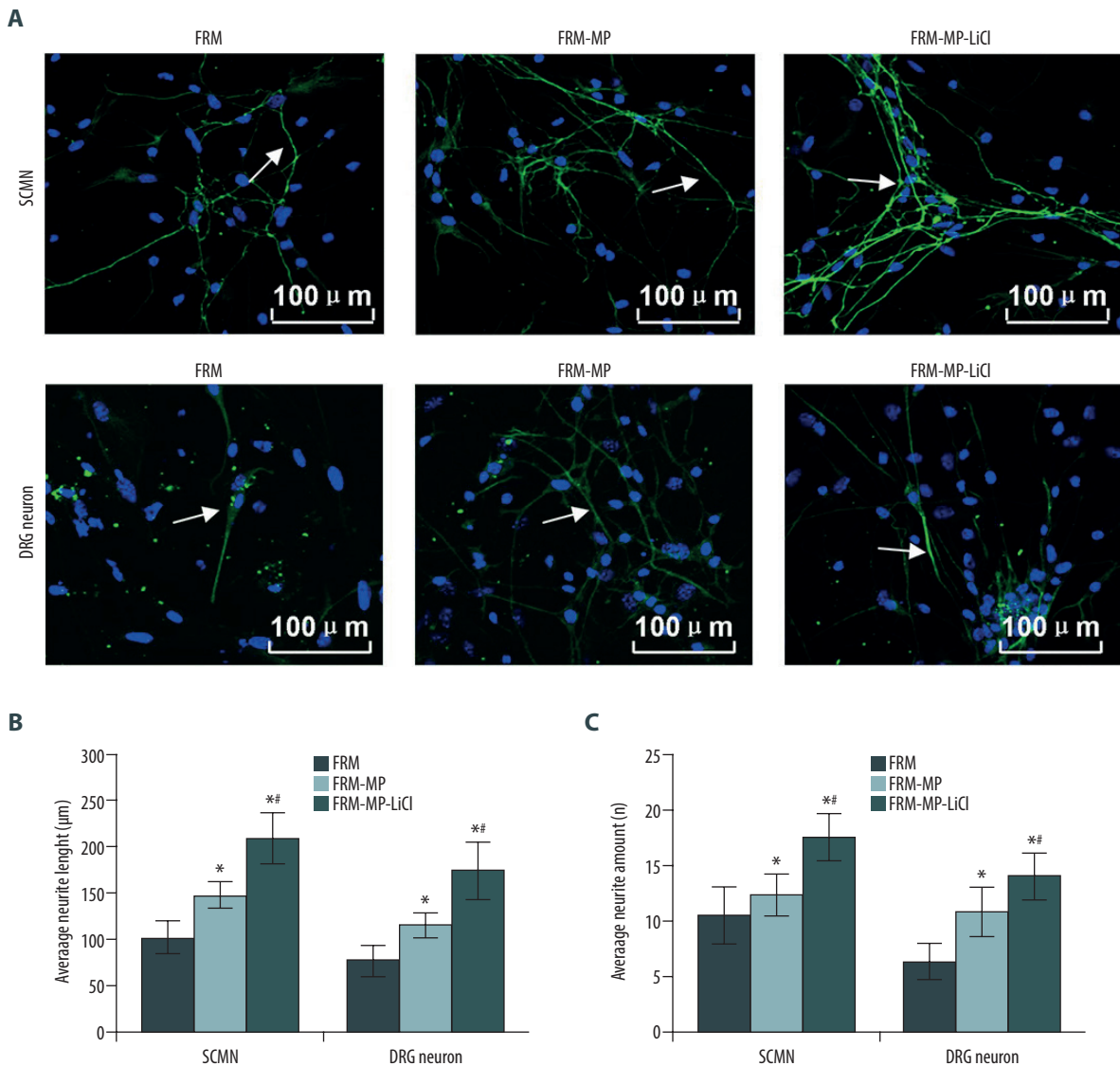


**Figure 5.** Measurement of neurite extension using immunofluorescence assay. (A) Measurement of neurite extension, including neurite length, amounts, and branches in SCMNs neurons and DRG neurons. (B) Statistical analysis of the length of neurite in SCMNs neurons and DRG neurons. (C) Statistical analysis of amount of neurite in both SCMNs neurons and DRG neurons. The white arrows represent the neurite. The scale bars were added in the images. \* $p < 0.05$  vs. FRM group. #  $p < 0.05$  vs. FRM-MP group.

#### RADA16-FRM-MP-LiCl decreased phosphorylation of Tau

We assessed the p-Tau/Tau-associated signaling pathway using Western blot assay (Figure 7A). Our findings showed that FRM-MP-LiCl incubation remarkably decreased the ratio of p-Tau/Tau compared to that in the FRM and FRM-MP groups in DRG neurons (Figure 7B,  $p < 0.05$ ) and SCMNs neurons (Figure 7C,  $p < 0.05$ ). Furthermore, FRM-MP-LiCl incubation significantly decreased the ratio of p-Tau/Tau compared to that in the FRM-MP group in DRG (Figure 7B,  $p < 0.05$ ) and SCMNs (Figure 7C,  $p < 0.05$ ) neurons.

#### RADA16-FRM-MP-LiCl downregulated calpain

The cell proliferative process-associated molecule, calpain, was also examined using Western blot assay (Figure 8A). The results showed that calpain expression in the FRM-MP-LiCl and FRM-MP groups was significantly downregulated in DRG neurons (Figure 8B) and SCMNs neurons (Figure 8C) compared to that in the FRM group ( $p < 0.05$ ). Moreover, calpain levels were significantly lower in DRG neurons (Figure 8B) and SCMNs neurons (Figure 8C) of the FRM-MP-LiCl group compared to that of the FRM-MP group ( $p < 0.05$ ).

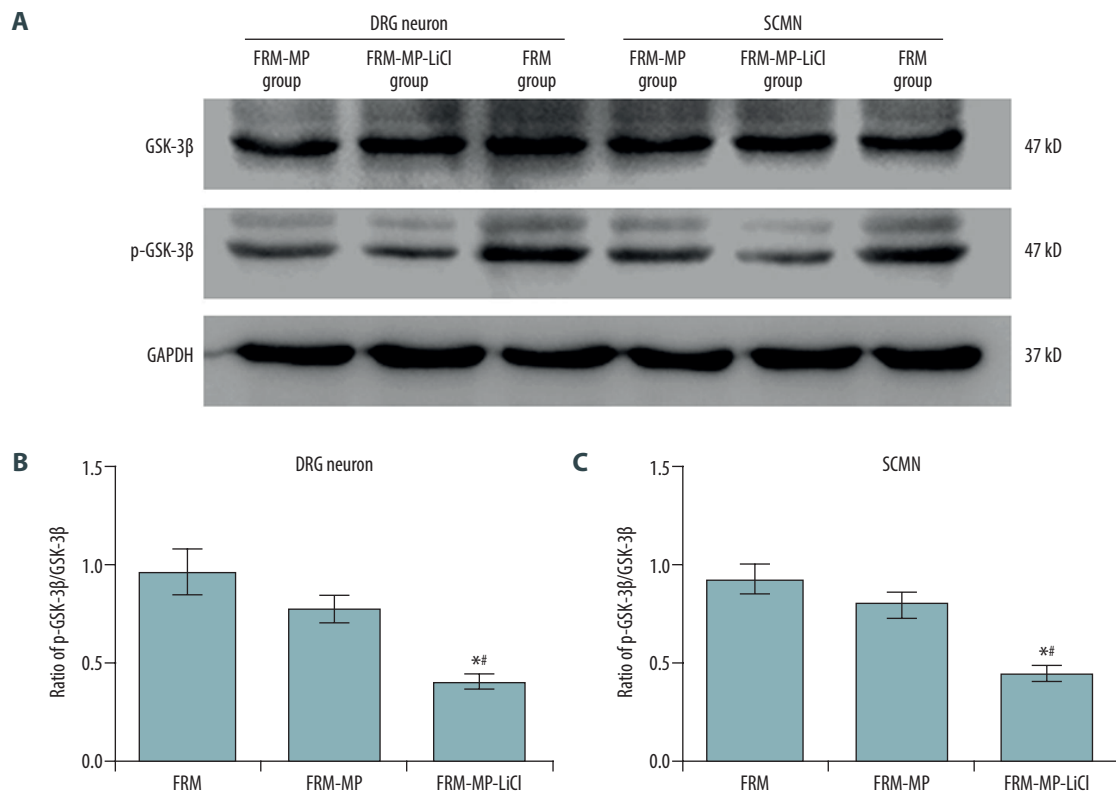


**Figure 6.** Determination of phosphorylated-GSK-3β (p-GSK-3β)/GSK-3β signaling pathway in neurons (DRG neurons and SCMN neurons) using Western blot assay. (A) Western blot images for GSK-3β and p-GSK-3β molecule expression in DRG neurons and SCMN neurons. (B) Statistical analysis of the ratio of p-GSK-3β/GSK-3β in DRG neurons. (C) Statistical analysis of the ratio of p-GSK-3β/GSK-3β in SCMN neurons. \*  $p < 0.05$  vs. FRM group. #  $p < 0.05$  vs. FRM-MP group.

## Discussion

The self-assembling peptide nano-fiber hydrogel presents possibility for the sustained and slow release of therapeutic molecules for treating disorders [19]. Self-assembling peptide hydrogel can also form three-dimensional pores with appropriate diameter of spherical-protein and can provide the optimal network structures for proliferation of cells [20,21]. Previous research reported that LiCl can trigger higher production of peptides and promote cell proliferation and differentiation [22,23]; therefore, we selected LiCl for use in a peptide-based nano-fiber scaffold in this study. We generated a RADA16 peptide-based nano-fiber scaffold containing SIDRVEPYSSSTAQ peptide (RADA16-FRM-MP), which was combined with LiCl to form a RADA16-FRM-MP-LiCl solution to incubate the neurons.

Release of multiple peptides (FRM peptide and FRM-MP peptide) from the RADA16-FRM and RADA16-FRM-MP hydrogels was slowed down day 1 to day 8, after which the level of release plateaued. In RADA16-FRM and RADA16-FRM-MP hydrogels, 100% peptide release has never been observed. In the present study, we isolated and identified the DRG neurons and

SCMN neurons to determine the effects of RADA16-FRM and RADA16-FRM-MP peptides on the proliferation and apoptosis of neurons. Our findings demonstrated that FRM-MP and FRM-MP-LiCl incubation both significantly enhanced cell proliferation and inhibited apoptosis of neurons compared to the FRM group, which suggests that the mimetic-peptide of SIDRVEPYSSSTAQ in the RADA16 scaffold plays critical role in promoting cell viability and inhibiting apoptosis. These results were consistent with a previous study [19], which reported that RADA16 self-assembling peptide facilitates formation of an appropriate microenvironment for cell proliferation. Previous studies [15,24] also reported that the self-assembling peptide hydrogels can resist degradation caused by natural proteases and can promote cell growth. Therefore, the RADA16 self-assembling peptide carrying a therapeutic molecule could be an ideal therapeutic strategy for repair or regeneration of damaged tissues.

Excepting for microenvironment for the cell proliferation, an optimal tissue-engineering scaffold should provide an appropriate micro-structure to modulate the adhesion of cells [25,26]. Our results indicated that the adherent ability of neurons in the FRM-MP and FRM-MP-LiCl incubation groups was significantly

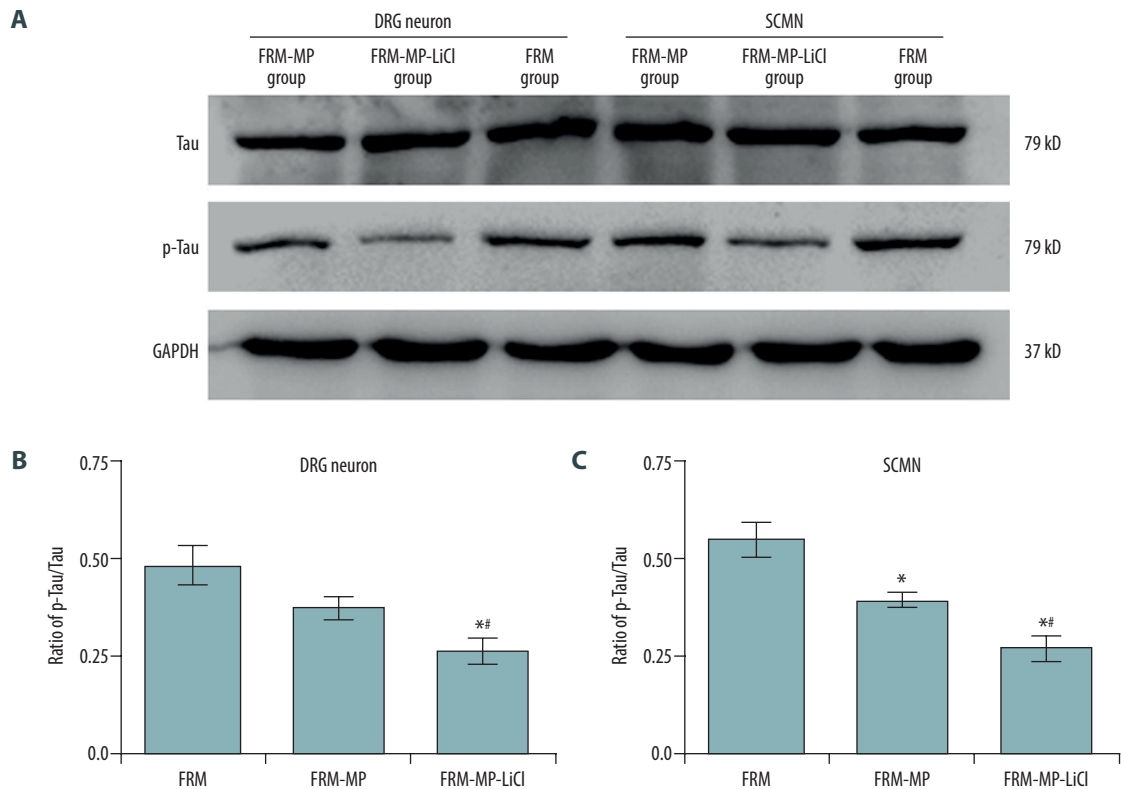


**Figure 7.** Examination for Tau and phosphorylated-Tau (p-Tau) expression in neurons (DRG neurons and SCMN neurons) using Western blot assay. (A) Western blot images for Tau and p-Tau molecule expression in DRG neurons and SCMN neurons. (B) Statistical analysis of ratio of p-GSK-3 $\beta$ /GSK-3 $\beta$  in DRG neurons. (C) Statistical analysis of ratio of p-GSK-3 $\beta$ /GSK-3 $\beta$  in SCMN neurons. \*  $p < 0.05$  vs. FRM group. #  $p < 0.05$  vs. FRM-MP group.

enhanced compared to that in the FRM group, especially for the FRM-MP-LiCl group, which had the highest adherence. These results suggest that the generated FRM-MP or FRM-MP-LiCl scaffold can promote cell-cell interactions, which is critical to tissue repair, such as neurite extension [27]. Therefore, we also determined the length, numbers, and branches of neurites in neurons. The results illustrated that the length of neurites and numbers of neurites were remarkably enhanced in the FRM-MP and FRM-MP-LiCl groups compared to that in the FRM group. LiCl incubation also enhanced the effects of FRM-MP (FRM-MP-LiCl) on neurite length and numbers. The SCMN and DRG neurons of the FRM-MP-LiCl group also had more neurite branches compared to that in the FRM and FRM-MP groups. This result suggests that RADA16 self-assembling peptide carried FRM peptide (SIDRVEPYSSTAQ) promotes the extension of neurites in neurons. Our cell adherence and neurite findings suggest that RADA16 self-assembling peptide-carried FRM is beneficial for the proliferation of neurons, and the LiCl microenvironment further promotes this effect. Lithium chloride (LiCl) has neuro-protective effects [28,29], which were also been shown by the present results.

GSK-3 $\beta$  is a serine/threonine protein kinase that can phosphorylate Tau protein in cultured cells *in vitro* [30,31]. Previous studies [32,33] reported that treating mice with GSK-3 $\beta$ -specific inhibitor significantly attenuates phosphorylation of Tau protein and prevents the Tau-induced neuro-degeneration. Calpain is a calcium-activated protease that can catalyze proteolytic cleavage [34]; it also participates in brain calcium homeostasis, and truncated calpain is associated with neuro-degenerative disorders [35, 36]. Therefore, both GSK-3 $\beta$  and calpain are believed to be associated with the abnormal phosphorylation of Tau protein and might play vital roles in neuro-degenerative disorders. Our findings demonstrated that FRM-MP-LiCl remarkably reduced phosphorylation of GSK-3 $\beta$  and Tau, and downregulated calpain in neurons. These results suggest that FRM-MP, especially for LiCl-incubated FRM-MP (FRM-MP-LiCl), has neuro-protective effects on neuron proliferation and extension by reducing phosphorylation of Tau through the calpain/GSK-3 $\beta$  signaling pathway [37].

Tau is a structural microtubule-related molecule that is extensively expressed in the nervous system and mediates neurite growth [38]. We speculate that the growth of neurites in SCMN

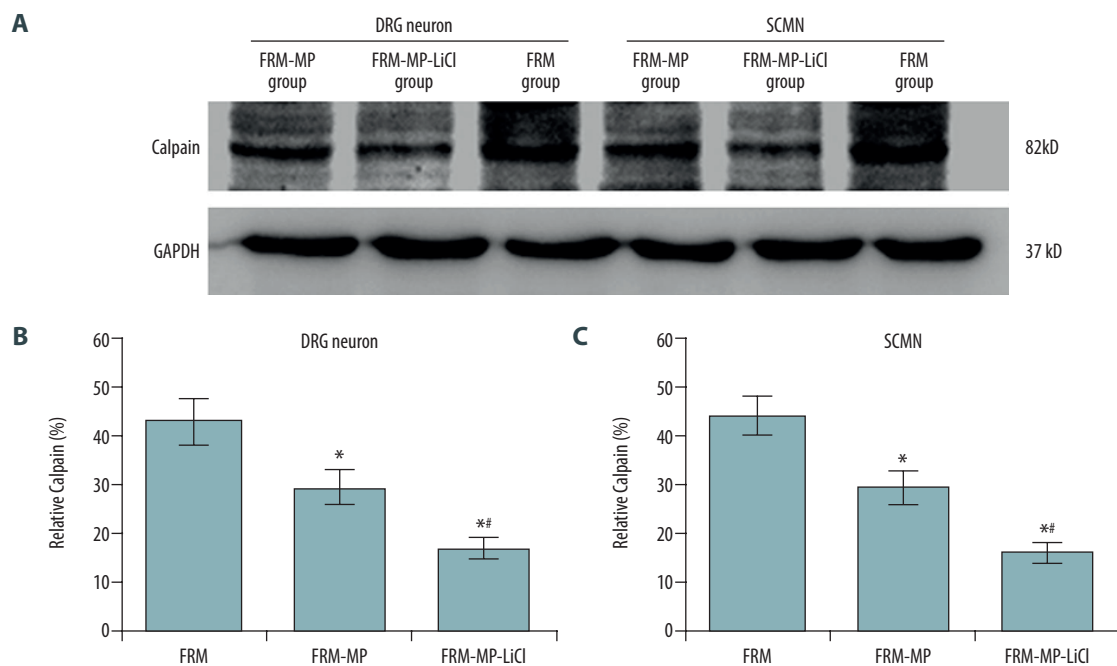


**Figure 8.** Effects of FRM-MP or FRM-MP-LiCl on calpain expression in neurons (DRG neurons and SCMN neurons) using Western blot assay. (A) Western blot images for the calpain expression. (B) Statistical analysis of calpain expression in DRG neurons. (C) Statistical analysis of calpain expression in SCMN neurons. \*  $p < 0.05$  vs. FRM group. #  $p < 0.05$  vs. FRM-MP group.

and DRG neurons is triggered by inhibiting the phosphorylation of Tau protein. LiCl is widely considered to inhibit GSK-3 $\beta$  activity and result in decreased phosphorylation of Tau. Therefore, FRM-MP-LiCl might promote the proliferation and growth of neurites through neural-cell adhesion molecule (NCAM)-derived mimetic-peptide (SIDRVEPYSSTAQ) and by downregulating Tau phosphorylation by LiCl. In future research, we plan to explore the physical characteristics and pharmacological mechanisms of RADA16-FRM-MP-LiCl.

## Conclusions

The generated self-assembling peptide scaffold-carrying FRM motif can remarkably promote neuron proliferation and adherent ability, inhibit apoptosis, and stimulate extension of neurites, by reducing phosphorylation of Tau protein through the calpain/GSK-3 $\beta$  signaling pathway. Our findings provide a novel mechanism of self-assembling peptide scaffold carrying FRM in the LiCl microenvironment, by which phosphorylation of Tau/GSK-3 $\beta$  and reduction of calpain are involved in neuro-degenerative disorders.

## Conflict of interest

None.

## References:

- Uhlir T, Kyprianou T, Martinelli FG et al: The emergence of peptides in the pharmaceutical business: From exploration to exploitation. *EuPA Open Proteom*, 2014; 4: 58–69
- Kotowski MJ, Bogacz A, Bartkowiak-Wieczorek J et al: Effect of multidrug-resistant 1 (MDR1) and CYP3A41B polymorphisms on cyclosporine-based immunosuppressive therapy in renal transplant patients. *Ann Transplant*, 2019; 24: 108–14
- Xiao YF, Jie MM, Li BS et al: Peptide-based treatment: A promising cancer therapy. *J Immunol Res*, 2015; 2015: 761820
- Bavec A: Peptide-based therapy for diabetes mellitus: Insulin versus incretins. *Life Sci*, 2014; 99: 7–13
- Gorbunov NV, Kiang JG: Ghrelin therapy decreases incidents of intracranial hemorrhage in mice after whole-body ionizing irradiation combined with burn trauma. *Int J Mol Sci*, 2017; 18: E1693
- Koss KM, Unsworth LD: Towards developing bioresponsive self-assembled peptide materials: Dynamic morphology and fractal nature of nanostructured matrices. *Materials (Basel)*, 2018; 11: E1539
- Tiwari G, Tiwari R, Sriwastawa B et al: Drug delivery systems: An updated review. *Int J Pharm Investig*, 2012; 2: 2–11
- Zhao X, Zhang S: Molecular designer self-assembling peptides. *Chem Soc Rev*, 2016; 35: 1105–10

9. Zhang S: Fabrication of the biomaterials through molecular self-assembly. *Nat Biotechnol*, 2003; 21: 1171–78
10. Johnson TD, Schristman KL: Injectable hydrogel therapies and their delivery strategies for treating myocardial infarction. *Expert Opin Drug Deliv*, 2013; 10: 59–72
11. Kim JK, Kim HJ, Chung JY et al: Natural and synthetic biomaterials for controlled drug delivery. *Arch Pharm Res*, 2014; 37: 60–68
12. Nishimura A, Hayakawa T, Yamamoto Y et al: Controlled release of insulin from self-assembling nanofiber hydrogel, PuraMatrix, application for the subcutaneous injection in rats. *Eur J Pharm Sci*, 2012; 45: 1–7
13. Koutsopoulos S, Zhang S: Long-term three-dimensional neural tissue cultures in functional self-assembling peptide hydrogels, matrigel and collagen I. *Acta Biomater*, 2013; 9: 5162–69
14. Kisiday J, Jin M, Kurz B et al: Self-assembling peptide hydrogel fosters chondrocyte extracellular matrix production and cell division: Implications for cartilage tissue repair. *Proc Natl Acad Sci USA*, 2002; 99: 9996–10001
15. Luo Z, He Y, Zhang Y et al: Designer D-form self-assembling peptide nanofiber scaffolds for 3-dimensional cell cultures. *Biomaterials*, 2013; 34: 4902–13
16. Zou Z, Liu T, Li J et al: Biocompatibility of functionalized designer self-assembling nanofiber scaffolds containing FRM motif for neural stem cells. *J Biomed Mater Res A*, 2014; 102: 1289–93
17. Shen H, Gan M, Yang H et al: An integrated cell isolation and purification method for rat dorsal ganglion neurons. *J Int Med Res*, 2019; 47: 3253–60
18. Montoya-Gacharna JV, Sutachan JJ, Chan WS et al: Preparation of adult spinal cord motor neuron cultures under serum-free conditions. *Methods Mol Biol*, 2012; 846: 1103–16
19. Zhou A, Chen S, He B et al: Controlled release of TGF-beta 1 from RADA self-assembling peptide hydrogel scaffolds. *Drug Des Devel Ther*, 2016; 10: 3043–51
20. Li Q, Chow KL, Chau Y: Three-dimensional self-assembling peptide matrix enhances the formation of embryoid bodies and their neuronal differentiation. *J Biomed Mater Res A*, 2014; 102: 1991–2000
21. Castells-Sala C, Recha-Sancho L, Lluçia-Valdeperas A et al: Three-dimensional cultures of human subcutaneous adipose tissue-derived progenitor cells based on RAD16-I self-assembling peptide. *Tissue Eng Part C Methods*, 2016; 22: 113–24
22. Brun O, Archibald LJ, Agramunt J et al: Simultaneous cyclization and derivatization of peptides using cyclopentenediones. *Org Lett*, 2017; 19: 992–95
23. Rattanawarawipa P, Pavasant P, Osathanon T et al: Effect of lithium chloride on cell proliferation and osteogenic differentiation in stem cells from human exfoliated deciduous teeth. *Tissue Cell*, 2016; 48: 425–31
24. Luo Z, Zhao X, Zhang S: Self-organization of a chiral D-EAK16 designer peptide into a 3D nanofiber scaffold. *Macromol Biosci*, 2008; 8: 785–91
25. Nune M, Kumaraswamy P, Krishnan UM et al: Self-assembling peptide nanofibrous scaffolds for tissue engineering: Novel approaches and strategies for effective functional regeneration. *Curr Protein Pept Sci*, 2013; 14: 70–84
26. Bergmeister H, Schreiber C, Grasl C et al: Healing characteristics of electrospun polyurethane grafts with various porosities. *Acta Biomater*, 2013; 9: 6032–40
27. Zhang S: Fabrication of the novel biomaterials through molecular self-assembly. *Nat Biotechnol*, 2003; 21: 1171–78
28. Qu N, Zhou XY, Han L et al: Combination of PPT with LiCl treatment prevented bilateral ovariectomy-induced hippocampal-dependent cognition deficit in rats. *Mol Neurobiol*, 2016; 53: 894–904
29. Carter ME, Han S, Palmiter RD: Parabrachial calcitonin gene-related peptide neurons mediate conditioned taste aversion. *J Neurosci*, 2015; 35: 4582–86
30. Peng H, Wang HB, Wang L et al: GSK-3 $\beta$  aggravates the depression symptoms in chronic stress mouse model. *J Integr Neurosci*, 2018; 17: 169–75
31. Liu F, Iqbal K, Grundke-Iqbal I et al: Involvement of aberrant glycosylation in phosphorylation of tau by cdk5 and GSK-3 $\beta$ . *FEBS Lett*, 2002; 530: 209–14
32. Noble W, Planel E, Zehr C et al: Inhibition of glycogen synthase kinase-3 by lithium correlates with reduced tauopathy and degeneration *in vivo*. *Proc Natl Acad Sci USA*, 2005; 102: 6990–95
33. Caccamo A, Oddo S, Tran LX et al: Lithium reduces tau phosphorylation but not A beta or working memory deficits in a transgenic model with both plaques and tangles. *Am J Pathol*, 2007; 170: 1669–75
34. Goll DE, Thompson VF, Li H et al: The calpain system. *Physiol Rev*, 2003; 83: 731–801
35. Veeranna, Kaji T, Boland B et al: Calpain mediates calcium-induced activation of the erk1/2 MAPK pathway and cytoskeletal phosphorylation in neurons: Relevance to Alzheimer's disease. *Am J Pathol*, 2004; 165: 795–805
36. Liu F, Grundke-Iqbal I, Iqbal K et al: Truncation and activation of calcineurin A by calpain I in Alzheimer disease brain. *J Biol Chem*, 2005; 280: 37755–62
37. Ma XH, Duan WJ, Mo YS et al: Neuroprotective effect of paeoniflorin on okadaic acid-induced tau hyperphosphorylation via calpain/Akt/GSK-3 $\beta$  pathway in SH-SY5Y cells. *Brain Res*, 2018; 1690: 1011
38. Cook B, Proctor D, Bromberg R et al: Digital quantification of neurite outgrowth and retraction by phase-contrast microscopy: A tau perspective. *Methods Cell Biol*, 2017; 141: 217–28